Structure
Ways & Means

Direct Visualization of HIV-1 with Correlative Live-Cell Microscopy and Cryo-Electron Tomography

Sangmi Jun,[1] Danxia Ke,[1] Karl Debiec,[1] Gongpu Zhao,[1] Xin Meng,[1] Zandrea Ambrose,[2] Gregory A. Gibson,[3] Simon C. Watkins,[3] and Peijun Zhang[1,*]
[1]Department of Structural Biology
[2]Division of Infectious Diseases, Department of Medicine
[3]Department of Cell Biology and Physiology
University of Pittsburgh School of Medicine, Pittsburgh, PA 15260, USA
*Correspondence: pez7@pitt.edu
DOI 10.1016/j.str.2011.09.006

SUMMARY

Cryo-electron tomography (cryoET) allows 3D visualization of cellular structures at molecular resolution in a close-to-native state and therefore has the potential to help elucidate early events of HIV-1 infection in host cells. However, structural details of infecting HIV-1 have not been observed, due to technological challenges in working with rare and dynamic HIV-1 particles in human cells. Here, we report structural analysis of HIV-1 and host-cell interactions by means of a correlative high-speed 3D live-cell-imaging and cryoET method. Using this method, we showed under near-native conditions that intact hyperstable mutant HIV-1 cores are released into the cytoplasm of host cells. We further obtained direct evidence to suggest that a hyperstable mutant capsid, E45A, showed delayed capsid disassembly compared to the wild-type capsid. Together, these results demonstrate the advantages of our correlative live-cell and cryoET approach for imaging dynamic processes, such as viral infection.

INTRODUCTION

Following fusion of the viral and host membranes, the HIV-1 capsid core is released into the cytoplasm of the host cell. The viral capsid disassembles in a process termed uncoating, and reverse transcription of the viral genome takes place (Freed, 1998; Aiken, 2006; Ganser-Pornillos et al., 2008). Uncoating is an essential yet poorly understood process that is generally assumed to occur rapidly and spontaneously (Grewe et al., 1990; Miller et al., 1997). Previous studies of the early stages of HIV-1 infection primarily employed live-cell fluorescence imaging to gain insight into the many steps of the HIV-1 life cycle (McDonald et al., 2002; Arhel et al., 2006; Jouvenet et al., 2008; Koch et al., 2009), revealing specific interactions between viral components and cellular factors (Maertens et al., 2005; Wu et al., 2006). However, the structural details underlying these steps, particularly disassembly of the viral core, are poorly defined.

Cryo-electron tomography (cryoET) has the potential to fill some critical gaps in our understanding of HIV-1: cryoET allows three-dimensional (3D) visualization of cellular structural details at nanometer resolution in a near-native state (Leis et al., 2009). It has provided a wealth of ultrastructural information on cellular compartments (Medalia et al., 2002; Cyrklaff et al., 2007; Zhang et al., 2007; Maurer et al., 2008; Patla et al., 2010) and purified or abundantly budding virus particles (Briggs et al., 2003; Grünewald et al., 2003; Cyrklaff et al., 2005; Cardone et al., 2007; Wright et al., 2007; Carlson et al., 2010). However, due to the poor signal, low contrast, and radiation sensitivity of unstained, frozen-hydrated specimens, acquisition of cryoET data for a selected target of interest, such as the site where HIV-1 enters the host cell, is often difficult. One critical challenge is that the specimen is ruined by radiation exposure before one finds the tiny region of interest in a relatively large cellular milieu. This is exacerbated when the method is applied to HIV-1 because productive infection is a relatively rare and dynamic event. On the other hand, fluorescence microscopy can be used to follow the dynamics of a viral particle, but the method lacks sufficient resolution to obtain a detailed understanding of events. Therefore, approaches for combining live-cell fluorescence light microscopy and cryoET are highly desirable, not only to complement the structural information obtained from cryoET with the dynamic, functional data from fluorescence labeling but also to accurately guide spatial and temporal sampling in cryoET.

Preparation for and imaging of samples by correlative light microscopy and cryoET pose many technical challenges (Plitzko et al., 2009), but the pioneering work of Plitzko and colleagues and others has demonstrated the feasibility of such experiments with cultured neurons, keratinocytes, and mitochondria (Sartori et al., 2007; Schwartz et al., 2007; Berriman et al., 2009; van Driel et al., 2009; Rigort et al., 2010). In their work, correlative methods were generally applied to guide the selection of regions of interest for cryoET data acquisition of large and static structures, and thus the methods were not suitable for the study of dynamic, diffraction-limited virus particles and interactions between these particles and cells at the early stages of infection. Here, we report the development of a new correlative method that extends the

correlative capability to a temporal dimension by using high-speed confocal live-cell imaging and cryoET. We applied this method not only to locate the object of interest for cryoET data collection, as previously reported for static objects, but also to characterize the spatial and temporal behavior of specific HIV-1 particles in living cells and to explore the structural details of virus-cell interactions at stages defined by live-cell analysis. Using the correlative 3D live-cell and cryoET approach, we directly observed HIV-1 particles (~100 nm in diameter) interacting with HeLa cells at different stages of infection, prior to and after membrane fusion. Using a hyperstable capsid mutant, E45A, we further show intact HIV-1 cores released into the cytoplasm after membrane fusion.

RESULTS

Cryofluorescence Light Microscopy Stage: Design and Performance

Our goal is to link high-resolution 3D structures of virus-host cell complexes to the dynamics of viral particles by correlating high-speed 3D live-cell imaging with high-resolution 3D cryoET. CryoET requires accurate localization of the site for data collection, since recording a full tilt series typically takes 1–2 hr without prior confirmation that the target has been captured. Although it is possible to correlate the last fluorescence confocal image in a live-cell series with cryoET for stationary viral particles, the time lapse of about 2–5 min between the last confocal live-cell image and plunge-freezing might be long enough for the position of the fluorescent particle to change due to the movement of either the cell or the particle itself. Thus, to facilitate cryoET data acquisition for high-resolution 3D structure analysis, we designed and built a cryofluorescence light microscopy stage (Figure 1) for imaging frozen-hydrated samples. The use of the cryostage allows a direct correlation between fluorescence signals and cryoET data, since the specimen is immobilized by cryofixation when fluorescence images are recorded. One distinct advantage of our stage design over previous ones (Sartori et al., 2007; Schwartz et al., 2007; van Driel et al., 2009; Rigort et al., 2010; Carlson and Evans, 2011) is the integrated specimen holder, which allows both light and electron microscopies to be performed on the same holder without specimen transfer. More specifically, the cryo-electron microscopy (cryoEM) grid remains in a single specimen cartridge during both fluorescence light microscopy and cryoEM analysis, thus minimizing any risk of specimen damage during grid transfer. This feature greatly enhances the performance of cryoET, since the flatness and integrity of the grid are critical for successful acquisition of cryoET data.

The homebuilt cryostage is quite simple and convenient to use. It includes a self-pressurized filling Dewar connecting to the liquid nitrogen inlet (Figure 1A, tubing 1), a liquid nitrogen overflow outlet (Figure 1A, tubing 2), and a dry nitrogen gas line to a sleeve over the objective lens to keep the lens warm and free of frost (Figure 1A, tubing 3). The specimen cartridge resides in an inner copper chamber and is cooled by the copper block and cold nitrogen gas. Therefore, the specimen remains stable for imaging even during refilling of liquid nitrogen. We characterized the cooling profile of the cryostage when it was mounted on the light microscope. As shown in Figure 1E, the temperature measured at the specimen cartridge reached −171°C within 4 min and stabilized at −187°C in about 6 min. The specimen remained steady for imaging during each refill, which occurred typically every 10–15 min (arrows in Figure 1E). The cryostage permitted cryofluorescence imaging for up to approximately 4 hr, allowing several cartridge exchanges. The optical resolution of the fluorescence microscope (van Driel et al., 2009) with the cryostage was about 0.6 μm, as measured using both GFP-tagged HIV-1 particles and quantum dots (Molecular Probes Inc.) (Figures 1F and 1G). Thus, fluorescent particles can be accurately localized into the cryoET imaging frame which is typically 2 μm × 2 μm in size.

Direct Visualization of Single HIV-1 Particles within an Infected HeLa Cell Using Correlative Light Microscopy and Cryo-Electron Microscopy

We first evaluated whether diffraction-limited small viral particles within an infected HeLa cell could be localized by fluorescence light microscopy and then directly visualized with cryoEM. To that end, HIV-1 virions, pseudotyped with the envelope glycoprotein of vesicular stomatitis virus (VSV-G) and containing GFP fused to HIV-1 Vpr (GFP-Vpr), were directly added to the HeLa cells cultured on carbon-coated EM finder grids (Figure 2A) at 17 hr after plating when the cells had been through one division and were mostly spread (see Movie S1 available online). After 20 min of exposure to the virus at room temperature, to allow viral attachment, cells were washed to remove unbound virus and supplemented with fresh media. After an additional 2 hr of incubation at 37°C, over 90% of the fluorescent particles were associated with HeLa cells (Figure S1), with several fluorescent particles visible in or on each HeLa cell (Figure 2C and inset). The majority of the fluorescent particles appeared to have ventured toward inner regions of the cell after 2 hr of incubation (Figure S1).

A major hurdle for imaging small particles, such as HIV-1, in cells by cryoEM is the limited field of view (~2 μm × 2 μm); HIV-1 particles are not abundant and are localized only to some regions of the cell. Thus, identifying a small region of interest in a ~50–100 μm wide cell represents a significant spatial challenge. We therefore used fluorescence light microscopy to localize the viral particles and guide cryoEM imaging for direct visualization of HeLa cell-associated HIV-1. After recording fluorescence images, we immediately preserved the EM grid in vitreous ice by plunge-freezing in liquid ethane (Dubochet et al., 1988). With an EM finder grid, the same grid square and cell that were imaged by fluorescence light microscopy were readily identified with cryoEM at a low magnification (Figures 2A, 2B, and 2D, red squares). Generally, individual fluorescent particles were localized with a precision better than 1 μm (Figures 1F and 1G), which is within the field of view for cryoEM imaging. After identification of GFP signals located in the thin peripheral area of cells and also in the vitreous ice-covered holes in the grid (Figures 2C and 2D, boxed areas), cryoEM analysis was carried out first by recording a low-dose projection image at a medium magnification (3500×) (Figure 2E). This step facilitated the precise localization of an identified region in the EM field for recording a high-magnification image (50,000×) (Figure 2F). The total electron dose applied to the low- and medium-magnification survey images was <1% of the dose

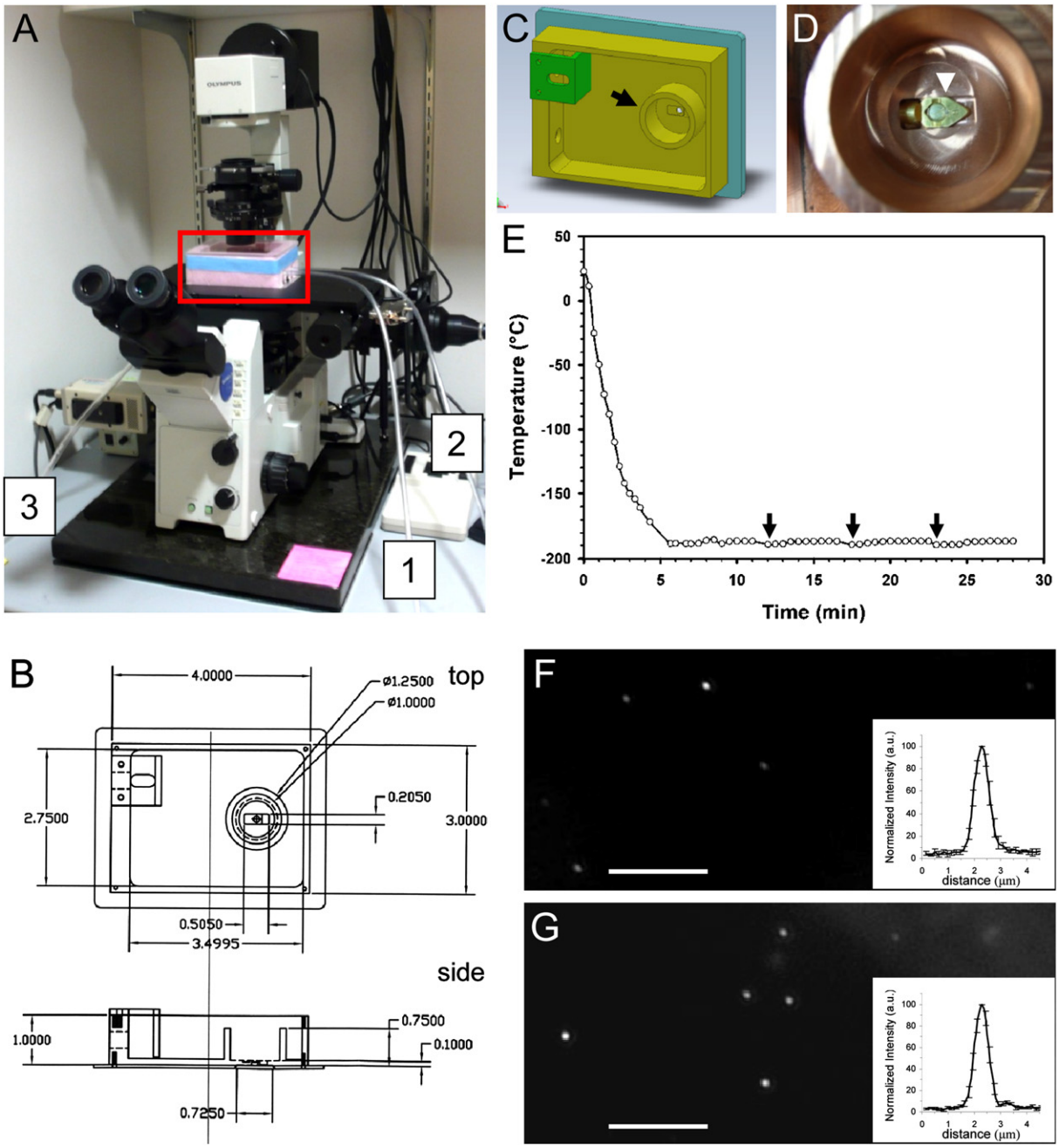

Figure 1. Construction and Characterization of the Cryofluorescence Light Microscopy Stage

(A) An overview of the cryostage (red box) mounted on an Olympus IX71 fluorescence light microscope. The three labeled tubes are for liquid nitrogen input (1), liquid nitrogen overflow protection (2), and dry nitrogen gas flow to the objective lens (3).

(B) AutoCAD drawings of the cryostage as viewed from the top and side. Dimensions are marked in inches.

(C) A 3D drawing of the cryostage sample chamber. The cartridge containing the electron microscopy grid is placed in the inner chamber (arrow).

(D) An enlarged photo of the inner chamber with an actual specimen cartridge (arrowhead).

(E) Cooling profile of the cryostage measured on the specimen cartridge. The arrows indicate the times when filling of liquid nitrogen from a pressurized tank occurred. The cartridge reaches −171°C within 4 min and stabilizes at −187°C within 6 min.

(F and G) Fluorescence images of GFP-tagged HIV-1 particles (F) and quantum dots (G) (acquisition time 10 s). Scale bar, 10 μm. Inserts depict the average of normalized intensity profiles of 10 particles. Error bars correspond to the standard deviation of the mean.

used in the final recording (20 e^{-}/Å^2). The HIV-1 particle, shown in Figure 2F, was found in a structure resembling a multivesicular body and displayed a clear conical capsid enclosed by an envelope (black arrow), suggesting that the particle likely had entered the cell via endocytosis and had not undergone membrane fusion with the endosome, consistent with previous results

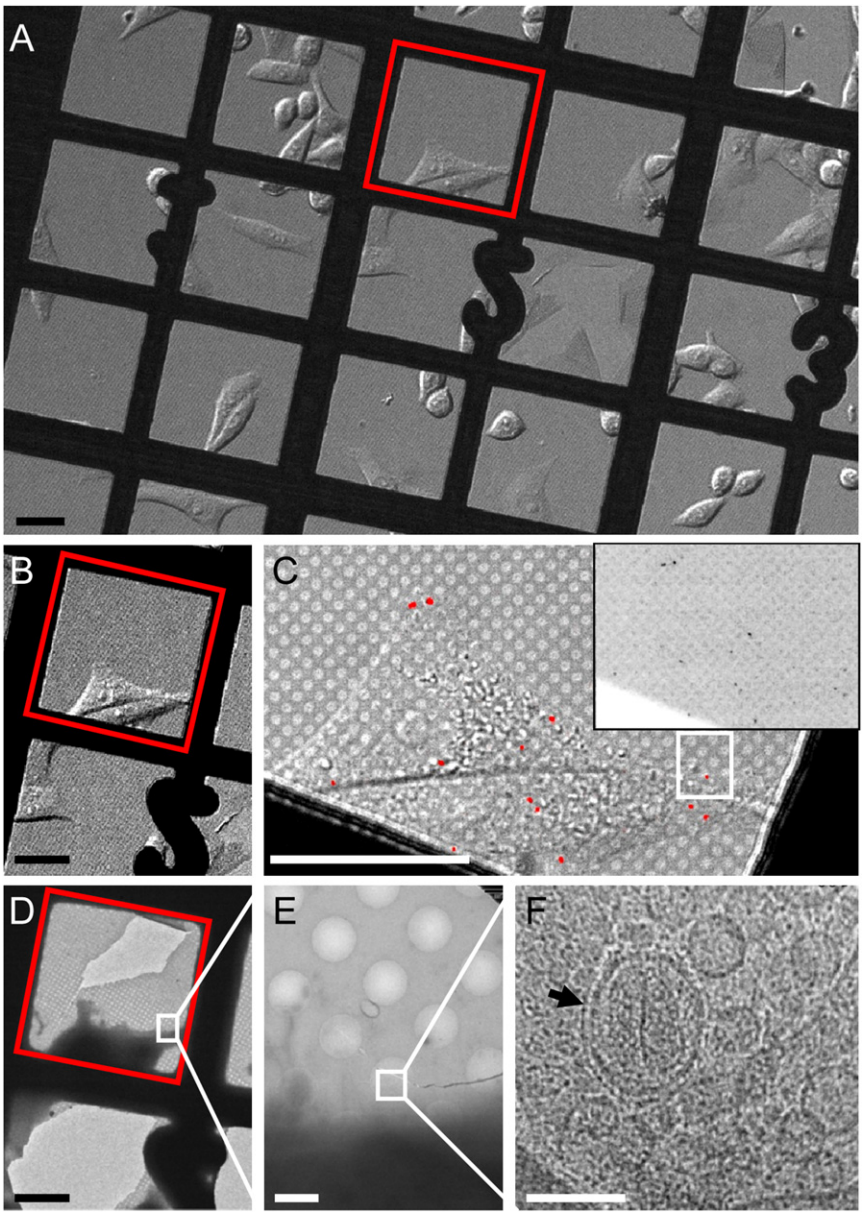

Figure 2. Cryo-Electron Microscopy (cryoEM) Imaging of Single HIV-1 Particles within a HeLa Cell by Correlative Microscopy

(A) An overview differential interference contrast (DIC) image (10×) of HeLa cells cultured on an index gold electron microscopy grid and infected with HIV-1 particles pseudotyped with the envelope glycoprotein of vesicular stomatitis virus and containing GFP-Vpr.

(B and C) DIC images of a selected area (red box in A) recorded with a 10× (B) or 60× (C) objective lens. Inset in C shows the raw GFP signals that were pseudocolored in red and overlaid on the DIC image in (C).

(D–F) Low-dose cryoEM images of the corresponding region in the DIC image (white box in [C]) containing a single GFP-labeled virus particle at nominal magnifications of 170× (D), 3500× (E), and 50,000× (F). The boxed region corresponds to the image frame in the adjacent panel. In (F), an HIV-1 particle with a conical core (arrow) is clearly visible inside a multivesicular body. Scale bars: 50 μm in (A)–(D), 2 μm in (E), and 0.1 μm in (F).

See also Movie S1 and Figure S1.

obtained using VSV-G pseudotyped HIV-1 virions (McDonald et al., 2002; Arhel et al., 2006; Miyauchi et al., 2009). The multivesicular body-like compartment contained many other vesicles of varying sizes.

Correlating HIV-1 Dynamics to Cellular Structures

To characterize the dynamic behavior of HIV-1 particles during the early stages of infection, HeLa cells infected with HIV-1 were imaged by high-speed confocal live-cell microscopy during the first 40 min after addition of viruses and prior to plunge-freezing. Time-lapse confocal images were collected at 1–2 min intervals from GFP-positive locations, identified prior to data acquisition. HIV-1 particle movements were analyzed by automated 3D particle tracking over time (Figures S2 and S3). Some viral particles moved rapidly in the cell from the cell periphery toward the perinuclear area in curvilinear paths (Figures S2, white trace, and S3A, blue trace), presumably through microtubule-based motors (McDonald et al., 2002; Arhel et al., 2006). At the same time, other particles remained stationary, typically appearing to move only 1–2 μm over the same time period (Figure S3A, red trace). We initially focused our cryoEM analysis on the stationary particles located near the cell periphery where the specimen was thin enough for transmission electron microscopy imaging. Since there was little movement of these particles, the confocal fluorescence image from the last time point could be directly used to guide cryoEM imaging. The HIV-1 particle (Figure S3A, red trace) that showed little movement stayed near a cellular protrusion for about 30 min before plunge-freezing. CryoEM projection images of the correlated region were first obtained at low and medium magnification (Figures S3B and S3C, respectively) to locate the area of interest. The subsequent high-magnification image (Figure S3D) showed that an intact HIV-1 particle was associated with a thin cellular protrusion that was suspended in a vitreous ice-covered hole. These and later (Figure 3) data suggest that such stationary HIV-1 particles likely remain bound to the plasma membrane and have not undergone membrane fusion or internalization into the cell. As displayed in the enlarged view of the particle in Figure S3E, the viral membrane and its enclosed viral core were clearly visible, with an oblique view of the viral capsid.

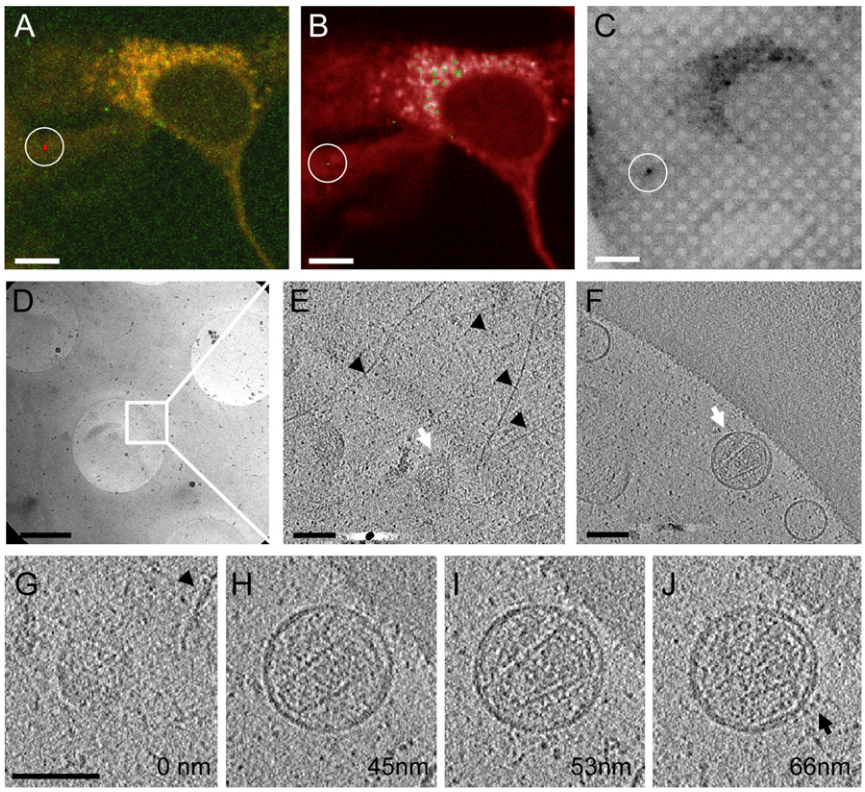

Figure 3. 3D Cryo-Tomographic Analysis of a Single Wild-Type HIV-1 Particle Bound to a HeLa Cell

(A) 3D tracking (red trace) of an HIV-1 particle over a period of 28 min, superimposed on the fluorescence image of HeLa cells from a confocal series taken at the last time point.

(B) A single z slice from the confocal series at the last time point overlaid with the HIV-1 GFP signals.

(C) Cryofluorescence image of the identical region displayed in (B) superimposed on a cryo-differential interference contrast image recorded after plunge-freezing.

(D–F) A low-dose cryo-electron microscopy image at 3500× (D) from the correlated region (circled in C), and tomographic slices (E and F) from the boxed area in (D). The upper slice (E) is near the bottom of the HeLa cell, whereas the lower slice (F), containing a virus particle, is located directly underneath the cell surface.

(G–J) Four 4 nm thick tomographic slices taken at the indicated relative z height from the tomogram. In (E) and (G), arrowheads point to intracellular filamentous structures; in (E) and (F), white arrows point to the HIV-1 particle; and in (J), the arrow indicates the viral envelope proteins. Scale bars: 10 μm in (A)–(C), 1 μm in (D), and 0.1 μm in (E)–(G). See also Movie S2 and Figures S2 and S3.

3D Structural Analysis of Dynamically Tracked HIV-1 Particles by Cryo-Electron Tomography

To directly link the 3D structures to the dynamics of viral particles, the movement of HIV-1 particles was followed by live-cell imaging for about 40 min immediately after addition of viruses (Figure 3A, red trace). Target particles selected for 3D analysis were located by correlation between the last fluorescence image of the live-cell series (Figure 3B, circled particle), the cryofluorescence image after plunge-freezing, obtained using our homebuilt cryostage (Figure 3C, circled particle), and the cryoEM image taken at a low magnification (Figure 3D). At the chosen site, a tilted projection series, from −70° to 70°, was recorded for reconstruction of a 3D tomogram (Figures 3E and 3F). The resulting 3D structure revealed an HIV-1 particle that had a clear conical core and was attached to the bottom surface of a HeLa cell (see Movie S2). Filamentous structures above the viral particle were visible in the tomographic slices of the HeLa cell (Figures 3E and 3G, black arrowheads), indicating that actin and other intracellular components might be involved in internalization of HIV-1 virions, as suggested previously (McDonald et al., 2002; Pontow et al., 2004; Miyauchi et al., 2009). The measured diameters of the particle were ∼120 nm in the xy-plane and ∼110 nm in the z direction, consistent with previous analyses of isolated virions (Briggs et al., 2003). Structural features, such as the viral membrane and the lattice of capsid protein in the core, were seen in the tomogram (Figures 3H–3J). In addition, HIV-1 VSV-G envelope molecules were seen nonrandomly clustered at particular regions of the viral membrane (Figure 3J, black arrow).

The VSV-G pseudotyped HIV-1 virions are thought to enter host cells via the endocytotic pathway (Aiken, 1997; Miyauchi et al., 2009). Membrane fusion at the endosome releases the viral cores into the cytoplasm and leads to other early infection events. We found that many intracellular HIV-1 particles, identified by four-dimensional tracking with confocal live-cell imaging, remained in vesicular compartments similar to the one shown in Figure 2F. Among the 65 HeLa cell-associated fluorescent particles analyzed by cryoEM, 24 were single, intact virions, either bound to the cell surface or within vesicular compartments. The rest showed no distinct features for HIV-1 particles: neither membrane enveloped virions nor conical/rod-shaped cores. Further 3D tomographic analyses of an additional 18 fluorescent particles identified 8 particles bound to the cell surface, 1 in a vesicle, and 9 without any distinctive viral particle structure. Again, no conical cores were observed in cells from these 3D correlated tomograms recorded after 40 min of incubation with viruses. In fact, no intact wild-type HIV-1 core was observed in our cryoEM analysis, indicating that the HIV-1 capsid may disassemble quickly after membrane fusion.

HIV-1 Capsid Mutation E45A Delays Capsid Disassembly in HeLa Cells

Since we did not find intact wild-type HIV-1 cores in tomograms containing intracellular GFP signals, we decided to look at a previously characterized mutant with the E45A amino acid substitution in the capsid, a substitution that presumably yields more-stable cores compared to the wild-type (Forshey et al., 2002; Ganser-Pornillos et al., 2004). Using our correlative

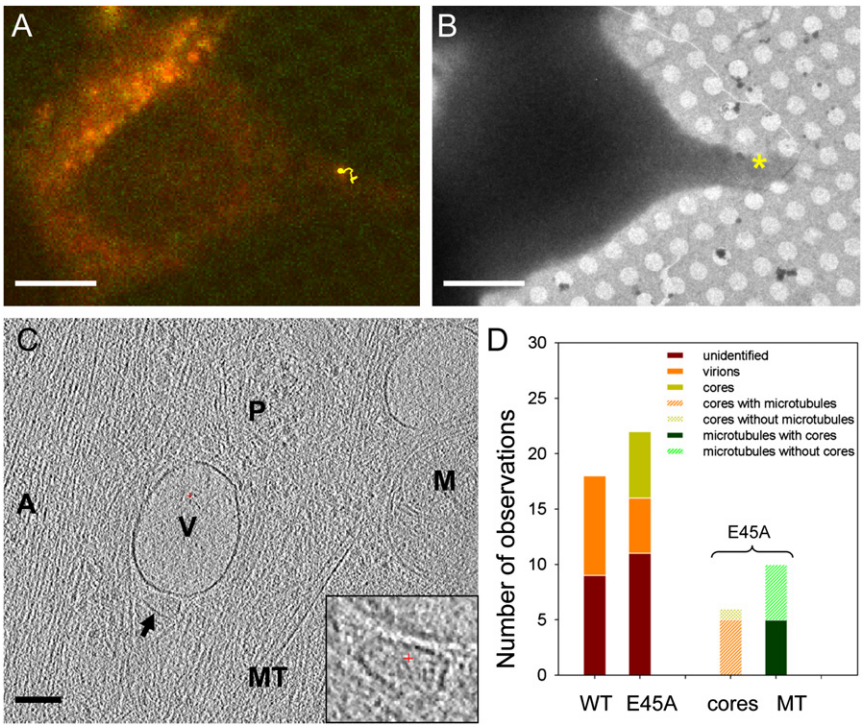

Figure 4. Direct Visualization of HIV-1 E45A Cores in HeLa Cells

(A) 3D tracking (yellow trace) of an HIV-1 E45A particle, overlaid on the last fluorescence image of HeLa cells in the time-lapse confocal series.

(B) A low-dose cryo-electron microscopy image of the correlated region taken at low magnification (3500×). The * indicates the location of the fluorescent particle.

(C) A 4 nm thick tomographic slice from the 3D tomogram of the correlated region of the HeLa cell. The arrow points to an HIV-1 viral core. A, actin filaments; MT, microtubule; V, vesicle; M, mitochondria; P, protein complexes. Inset, an enlarged view of the HIV-1 core structure.

(D) Quantitative analysis of the occurrence of HIV-1 virions and cores in cellular tomograms of infected HeLa cells. Scale bars: 10 μm in (A) and (B), 0.1 μm in (C). See also Figure S4.

method, we tracked and analyzed E45A virions in a manner similar to that used for the wild-type capsid virus. The optical behavior of E45A particles was similar to that of wild-type particles to some degree, displaying both stationary and directed movement toward the nucleus. Yet, conical cores, similar to the ones observed in isolated virions (Briggs et al., 2006), were clearly visible in several tomograms recorded from the areas containing intracellular GFP signals (Figure 4C, inset; Figure S4). In Figure 4A, live-cell imaging showed that the particle is, in fact, in the process of moving toward the nucleus. We observed intact cores in a 3D network of closely apposed membranous organelles, actin filaments, microtubules, and many protein complexes. The cores often appear associated with vesicles and actin filaments and in close proximity to microtubules (Figure 4C; Figure S4), suggesting that the intracellular trafficking network might be involved in directed core transport. Although the scanning electron microscopy image of intracellular HIV-1 capsid protein (CA) shells has been shown in fixed and dehydrated cells (Arhel et al., 2007), this is the first direct visualization of HIV-1 cores inside of a host cell in near-native conditions at high resolution.

Quantitative comparison of wild-type and E45A CA mutant HIV-1 infected cells indicates a striking difference between the particles (Figure 4D). Of the fluorescent wild-type capsid particles analyzed by cryoET (n = 18), 50% were enveloped virions. However, no individual intact viral core was found after careful examination of all tomograms. In contrast, of the fluorescent E45A HIV-1 particles examined (n = 22), 23% were enveloped, intact virions and 27% were cytoplasmic, conical cores. Microtubules were observed in 80% of the tomograms containing cytoplasmic HIV-1 cores, while actin filaments were always found next to the cores. Microtubules were also observed in half of the E45A HIV-1 tomograms containing GFP signals but no recognizable conical HIV-1 cores.

DISCUSSION

We used an advanced correlative approach to link time-lapse live-cell 3D fluorescence microscopy to cryoET, allowing direct visualization of early stages of HIV-1 infection. We observed stationary HIV-1 particles (~100 nm in diameter) attached to the plasma membrane at cellular protrusions or internalized in vesicular compartments, whereas moving particles appeared to be released into the cytoplasm after membrane fusion and en route to the nucleus. Cellular filaments were always found at the site where intact enveloped HIV-1 particles bind, prior to internalization. These findings confirm the results obtained from previous live-cell fluorescence imaging studies (McDonald et al., 2002; Arhel et al., 2006; Miyauchi et al., 2009) and extend the analysis to high-resolution 3D ultrastructure details. Our data further suggest that upon membrane fusion, the wild-type HIV-1 cores break down rather quickly, within ~40 min. This agrees with the half-life of ~23 min recently established by the Hope laboratory using an assay that measures the sensitivity of the wild-type cores to TRIM-Cyp restriction (Hulme et al., 2011). However, it is possible that the structure of the capsid is perturbed quickly but that complete uncoating (i.e., the complete shedding of the capsid) takes longer and occurs in multiple stages (Arhel et al., 2007, 2010; Hulme et al., 2011). A recent study reported that the half-life of escape of HIV-1 from the capsid inhibitor PF74 is approximately 4 hr, suggesting that uncoating could be slower (Blair et al., 2010). Additionally, our results support the conclusion that the capsid E45A mutation confers increased core stability (Forshey et al., 2002), as these particles undergo delayed capsid disassembly in target cells compared with wild-type HIV-1 under the same conditions.

In that our method examines particle dynamics within cells prior to correlative microscopy, the method represents an important advance over previous efforts aimed at developing techniques to correlate cryo-light microscopy and cryoEM (Sartori

et al., 2007; Schwartz et al., 2007; Berriman et al., 2009; van Driel et al., 2009; Rigort et al., 2010). With high-speed confocal live-cell light microscopy followed by cryofluorescence microscopy and cryoET, we are able to connect dynamic behavior of virus particles in time and space, in live cells, with the ultrastructure information acquired in the frozen-hydrated state, thus, allowing insights into the temporal and spatial relationship between viruses and host cells. Previous studies in this area did not incorporate a means to measure particle dynamics. Another advantage of our method is the simple cryostage with an integrated specimen holder, allowing sequential cryo-light microscopy and cryoEM on a single specimen holder without sample transfer, thus eliminating potential specimen damage during transfer. Although a Polara sample cartridge was incorporated in our design, other cryoET specimen carriages, including the Titan Krios AutoGrid sample holder, can be easily adapted. A limitation of our correlative approach, when applied to study virus infection, is the restricted accessibility of the cells in cryoET, due to their intrinsic thickness. The areas in the cell that can be investigated must be <0.5 μm thick. Even with cells spread out between mitosis phases, the accessible areas are still limited to the peripheral regions of the cells. Thus, only very early infection events are available for cryoET analysis using this method. To investigate viral particles in thicker areas, for instance near the nucleus, application of additional techniques, such as cryo-focused ion beam milling (Marko et al., 2007) or vitreous sectioning (Zhang et al., 2004), may be useful to reduce sample thickness, thus increasing the utility of the method described here.

Our results illustrate the potential of correlative microscopy for advancing the study of virus particle interactions with the host cell. Further labeling of cellular factors with a fusion tag that is visible to EM, such as tetracysteine-ReAsh (Gaietta et al., 2002), metallothionein (Mercogliano and DeRosier, 2007), or the recently reported ferritin-fusion tag (Wang et al., 2011), may facilitate the identification of specific stages of the HIV-1 life cycle that are uniquely associated with host proteins and the spatial relationship of these host factors with viral particles. This work represents our first step toward detailed 3D structural analysis of early stages of HIV-1 infection. We anticipate that the correlative method established here will not only constitute a useful tool for studying dynamic virus-host cell interplay at various stages during infection but also open new ways to investigate cell signaling events and many other cellular processes in general.

EXPERIMENTAL PROCEDURES

Production of VSV-G Pseudotyped HIV-1 Particles Containing GFP-Vpr

Wild-type and E45A HIV-1 particles were produced by transfecting 293T cells with three plasmids: pL-VSV-G (a kind gift from M. Emerman [Bartz and Vodicka, 1997]), peGFPC3-Vpr (a kind gift from T. Hope [McDonald et al., 2002]), and a proviral plasmid, pNLdVdE-luc, encoding HIV-1_{NL4-3} with deletions in *vpr* and *env* and with the luciferase gene in place of *nef*. Transfections were performed in 293T cells with Lipofectamine 2000 (Invitrogen, Carlsbad, CA) in Dulbecco's modified Eagle's medium (DMEM) containing 10% fetal bovine serum (Atlanta Biologicals, Lawrenceville, GA). Particle infectivity was determined on GHOST-R3/X4/R5 cells, and capsid levels were measured by p24 enzyme-linked immunosorbent assay (Zeptometrix, Buffalo, NY).

Cell Culture and HIV-1 Infection

HeLa cells were cultured at 37°C with 5% CO_2 in DMEM with 4.5 g/l L-glutamine and glucose (Lonza Group Ltd., Basel, Switzerland) containing 10% heat-inactivated fetal calf serum, 100 units/ml penicillin, and 100 μg/ml streptomycin (Invitrogen Corporation, Carlsbad, CA). Cultures at ~80% confluence were routinely split 1:5 in 60 mm culture dishes. Cells were centrifuged at 1000×g and plated onto the gold R2/2 Quantifoil finder EM grids (Quantifoil Micro Tools GmbH, Jena, Germany) at a density of 2 × 10^4 cells/ml (total 2 ml culture) in glass-bottom culture dishes (MatTek Corporation, Ashland, MA). The gold EM grids were disinfected under UV light for 2 hr and coated with 50 μg/ml fibronectin (Sigma, St. Louis, MO) before use. HeLa cell cultures were monitored in real time in situ with a VivaView FL Incubator Fluorescence Microscope (Olympus America, Inc., Center Valley, PA), to monitor cell division. Specifically, HeLa cells were cultured on carbon-coated EM finder grids (Figure 2A) and followed for a period of 20 hr by automatically collecting differential interference contrast images every 10 min, at multiple positions (Movie S1). The cells appeared to have an 18 hr division cycle when grown on EM grids and undergo a shape change when they divide, becoming spherical during mitosis and spreading thin afterwards (Movie S1). Since cryoEM requires relatively thin specimens, the optimal time window for cryoEM imaging is therefore at the midpoint between two mitosis phases, approximately 18 hr after plating, when the cells have been through one division and are mostly spread.

Cells were infected in culture medium with 20 μl of VSV-G pseudotyped HIV-1 containing GFP-Vpr (40 ng p24). For initial correlative analysis of viral particles, viruses were first incubated with cell culture for 20 min at room temperature to allow attachment. Cells were then washed with prewarmed fresh DMEM to remove unbound virus and further incubated for 2 hr before imaging. The fluorescence images (Figure 2; Figure S1) were acquired with a digital CCD camera and Olympus MetaMorph digital imaging software, using a 60×/1.35 NA oil immersion objective lens.

Live-Cell Imaging

Time-lapse confocal live-cell imaging was performed immediately after addition of viruses and identification of cells associated with GFP signals, by using a Tokai Hit (Tokyo, Japan) live-cell chamber at 37°C in a Nikon TiE microscope equipped with a Prairie Technologies sweptfield confocal microscope. Glass-bottom dishes containing HeLa cells cultured on EM grids were placed onto the microscope stage, and high-speed 3D images were acquired using a Photometrics Evolve camera, NIS-Elements software (Nikon Instruments, Melville, NY), and a 60×/1.35 NA oil immersion objective lens. Time-lapse confocal image stacks were collected for 40 min after addition of GFP-labeled HIV-1 virions. Image stacks were collected every 1 to 2 min and streamed to a large disk array. Data were analyzed using MetaMorph (Molecular Devices, Sunnyvale, CA) or Imaris (Bitplane, Zurich, Switzerland) software, and particles were tracked in two and three dimensions to measure the dynamics.

Cryofluorescence Light Microscopy

Immediately after fluorescence confocal live-cell imaging, 4 μl of 15 nm gold beads were applied to the EM grids to serve as fiducial markers for tomographic alignment. The grids were blotted with filter paper and plunged into liquid ethane for rapid vitrification using an FEI Vitrobot (FEI, Hillsboro, OR). Frozen-hydrated samples were placed in specimen cartridges and loaded into a homebuilt cryofluorescence sample stage, which was mounted on an Olympus IX71 microscope and cooled with liquid nitrogen to maintain the specimen temperature below −177°C. A dry nitrogen gas flow was fed to the objective lens during imaging to avoid frost build up. The images were acquired by using an Olympus LUCPlanFLN 40×/0.6 NA with a 2.7–4 mm working distance objective lens. The cryofluorescence light images were correlated with both fluorescence light images from live cells and cryoEM projection images at low and medium magnifications, facilitating a good grasp of the position of viruses for cryoET.

Cryo-Electron Microscopy and Cryo-Electron Tomography

Frozen EM grids were stored in liquid nitrogen before they were examined by cryoEM. The regions containing HIV-1 were first manually identified in EM projection images, taken at a low magnification (170×), by correlating with room temperature or cryofluorescence light microscope images. Low-dose

($20\ e^{-}/Å^2$) projection images of the identified regions of interest were recorded using a Tecnai F20 transmission electron microscope equipped with a field emission gun (FEI, Hillsboro, OR) and a Gatan 4K × 4K CCD camera (Gatan, Inc., Warrendale, PA) at a magnification of 50,000× and under-focus values ranging from 2 to 5 μm. For 3D cryoET, frozen-hydrated EM grids were placed in cartridges and loaded into the cryotransfer system of a Polara G3 microscope (FEI). The Polara microscope was equipped with a field emission gun operating at 200 kV and a Gatan GIF2000 energy filter. A series of low-dose projection images of the region of HeLa cells containing HIV-1 signals were recorded at a tilt angle range from −70° to 70° at a nominal magnification of 27,500× with under-focus values between 5 and 8 μm and a 20 eV energy filter slit. The total dose used for each tilt series was typically ~60–70 $e^{-}/Å^2$. Tilt series were aligned using 15 nm gold bead fiducial markers and were refined to standard deviations below 0.8. A weighted back-projection algorithm, as implemented in the IMOD reconstruction package (Kremer et al., 1996), was used to convert the information present in the series of tilted projection images into 3D density maps (tomograms). The 3D tomographic volumes were visualized in the environment of the program Amira (TGS Inc., San Diego, CA).

Tomograms were analyzed for HIV-1 virions, capsids, microtubules, and vesicular compartments. The numbers of observed virions, cores, and microtubules in tomograms were recorded. Potential areas of interest were denoised using a 3D nonlinear anisotropic diffusion edge enhancing program implemented in IMOD with 15 iterations and a *k* of 6.4, allowing clearer visualization.

SUPPLEMENTAL INFORMATION

Supplemental Information includes two movies and four figures and can be found with this article online at doi:10.1016/j.str.2011.09.006.

ACKNOWLEDGMENTS

The authors thank Dr. Sriram Subramaniam for use of the FEI Polara microscope in his facility; Travis Wheeler and the machine shop of the Department of Cell Biology and Physiology for construction of the cryofluorescence sample stage; Tamera Franks for technical assistance; and Drs. Christopher Aiken and Teresa Brosenitsch for critical reading of the manuscript. The authors also thank Michael Emerman and Tom Hope for plasmid constructs. This work is a contribution from the Pittsburgh Center for HIV Protein Interactions and was supported by the National Institutes of Health (GM082251, GM085043, and RR024424).

Received: May 17, 2011
Revised: September 13, 2011
Accepted: September 17, 2011
Published: November 8, 2011

REFERENCES

Aiken, C. (1997). Pseudotyping human immunodeficiency virus type 1 (HIV-1) by the glycoprotein of vesicular stomatitis virus targets HIV-1 entry to an endocytic pathway and suppresses both the requirement for Nef and the sensitivity to cyclosporin A. J. Virol. *71*, 5871–5877.

Aiken, C. (2006). Viral and cellular factors that regulate HIV-1 uncoating. Curr. Opin. HIV AIDS *1*, 194–199.

Arhel, N. (2010). Revisiting HIV-1 uncoating. Retrovirology *7*, 96–105.

Arhel, N., Genovesio, A., Kim, K.A., Miko, S., Perret, E., Olivo-Marin, J.C., Shorte, S., and Charneau, P. (2006). Quantitative four-dimensional tracking of cytoplasmic and nuclear HIV-1 complexes. Nat. Methods *3*, 817–824.

Arhel, N.J., Souquere-Besse, S., Munier, S., Souque, P., Guadagnini, S., Rutherford, S., Prévost, M.C., Allen, T.D., and Charneau, P. (2007). HIV-1 DNA Flap formation promotes uncoating of the pre-integration complex at the nuclear pore. EMBO J. *26*, 3025–3037.

Bartz, S.R., and Vodicka, M.A. (1997). Production of high-titer human immunodeficiency virus type 1 pseudotyped with vesicular stomatitis virus glycoprotein. Methods *12*, 337–342.

Berriman, J.A., Li, S., Hewlett, L.J., Wasilewski, S., Kiskin, F.N., Carter, T., Hannah, M.J., and Rosenthal, P.B. (2009). Structural organization of Weibel-Palade bodies revealed by cryo-EM of vitrified endothelial cells. Proc. Natl. Acad. Sci. USA *106*, 17407–17412.

Blair, W.S., Pickford, C., Irving, S.L., Brown, D.G., Anderson, M., Bazin, R., Cao, J., Ciaramella, G., Isaacson, J., Jackson, L., et al. (2010). HIV capsid is a tractable target for small molecule therapeutic intervention. PLoS Pathog. *6*, e1001220.

Briggs, J.A., Wilk, T., Welker, R., Kräusslich, H.G., and Fuller, S.D. (2003). Structural organization of authentic, mature HIV-1 virions and cores. EMBO J. *22*, 1707–1715.

Briggs, J.A., Grünewald, K., Glass, B., Förster, F., Kräusslich, H.G., and Fuller, S.D. (2006). The mechanism of HIV-1 core assembly: insights from three-dimensional reconstructions of authentic virions. Structure *14*, 15–20.

Cardone, G., Winkler, D.C., Trus, B.L., Cheng, N., Heuser, J.E., Newcomb, W.W., Brown, J.C., and Steven, A.C. (2007). Visualization of the herpes simplex virus portal in situ by cryo-electron tomography. Virology *361*, 426–434.

Carlson, D.B., and Evans, J.E. (2011). Low-cost cryo-light microscopy stage fabrication for correlated light/electron microscopy. J. Vis. Exp. *52*, e2909.

Carlson, L.A., de Marco, A., Oberwinkler, H., Habermann, A., Briggs, J.A., Kräusslich, H.G., and Grünewald, K. (2010). Cryo electron tomography of native HIV-1 budding sites. PLoS Pathog. *6*, e1001173.

Cyrklaff, M., Risco, C., Fernández, J.J., Jiménez, M.V., Estéban, M., Baumeister, W., and Carrascosa, J.L. (2005). Cryo-electron tomography of vaccinia virus. Proc. Natl. Acad. Sci. USA *102*, 2772–2777.

Cyrklaff, M., Linaroudis, A., Boicu, M., Chlanda, P., Baumeister, W., Griffiths, G., and Krijnse-Locker, J. (2007). Whole cell cryo-electron tomography reveals distinct disassembly intermediates of vaccinia virus. PLoS ONE *2*, e420.

Dubochet, J., Adrian, M., Chang, J.J., Homo, J.C., Lepault, J., McDowall, A.W., and Schultz, P. (1988). Cryo-electron microscopy of vitrified specimens. Q. Rev. Biophys. *21*, 129–228.

Forshey, B.M., von Schwedler, U., Sundquist, W.I., and Aiken, C. (2002). Formation of a human immunodeficiency virus type 1 core of optimal stability is crucial for viral replication. J. Virol. *76*, 5667–5677.

Freed, E.O. (1998). HIV-1 gag proteins: diverse functions in the virus life cycle. Virology *251*, 1–15.

Gaietta, G., Deerinck, T.J., Adams, S.R., Bouwer, J., Tour, O., Laird, D.W., Sosinsky, G.E., Tsien, R.Y., and Ellisman, M.H. (2002). Multicolor and electron microscopic imaging of connexin trafficking. Science *296*, 503–507.

Ganser-Pornillos, B.K., Yeager, M., and Sundquist, W.I. (2008). The structural biology of HIV assembly. Curr. Opin. Struct. Biol. *18*, 203–217.

Ganser-Pornillos, B.K., von Schwedler, U.K., Stray, K.M., Aiken, C., and Sundquist, W.I. (2004). Assembly properties of the human immunodeficiency virus type 1 CA protein. J. Virol. *78*, 2545–2552.

Grewe, C., Beck, A., and Gelderblom, H.R. (1990). HIV: early virus-cell interactions. J. Acquir. Immune Defic. Syndr. *3*, 965–974.

Grünewald, K., Desai, P., Winkler, D.C., Heymann, J.B., Belnap, D.M., Baumeister, W., and Steven, A.C. (2003). Three-dimensional structure of herpes simplex virus from cryo-electron tomography. Science *302*, 1396–1398.

Hulme, A.E., Perez, O., and Hope, T.J. (2011). Complementary assays reveal a relationship between HIV-1 uncoating and reverse transcription. Proc. Natl. Acad. Sci. USA *108*, 9975–9980.

Jouvenet, N., Bieniasz, P.D., and Simon, S.M. (2008). Imaging the biogenesis of individual HIV-1 virions in live cells. Nature *454*, 236–240.

Koch, P., Lampe, M., Godinez, W.J., Müller, B., Rohr, K., Kräusslich, H.G., and Lehmann, M.J. (2009). Visualizing fusion of pseudotyped HIV-1 particles in real time by live cell microscopy. Retrovirology *6*, 84–97.

Kremer, J.R., Mastronarde, D.N., and McIntosh, J.R. (1996). Computer visualization of three-dimensional image data using IMOD. J. Struct. Biol. *116*, 71–76.

Leis, A., Rockel, B., Andrees, L., and Baumeister, W. (2009). Visualizing cells at the nanoscale. Trends Biochem. Sci. *34*, 60–70.

Maertens, G., Vercammen, J., Debyser, Z., and Engelborghs, Y. (2005). Measuring protein-protein interactions inside living cells using single color fluorescence correlation spectroscopy. Application to human immunodeficiency virus type 1 integrase and LEDGF/p75. FASEB J. *19*, 1039–1041.

Marko, M., Hsieh, C., Schalek, R., Frank, J., and Mannella, C. (2007). Focused-ion-beam thinning of frozen-hydrated biological specimens for cryo-electron microscopy. Nat. Methods *4*, 215–217.

Maurer, U.E., Sodeik, B., and Grünewald, K. (2008). Native 3D intermediates of membrane fusion in herpes simplex virus 1 entry. Proc. Natl. Acad. Sci. USA *105*, 10559–10564.

McDonald, D., Vodicka, M.A., Lucero, G., Svitkina, T.M., Borisy, G.G., Emerman, M., and Hope, T.J. (2002). Visualization of the intracellular behavior of HIV in living cells. J. Cell Biol. *159*, 441–452.

Medalia, O., Weber, I., Frangakis, A.S., Nicastro, D., Gerisch, G., and Baumeister, W. (2002). Macromolecular architecture in eukaryotic cells visualized by cryoelectron tomography. Science *298*, 1209–1213.

Mercogliano, C.P., and DeRosier, D.J. (2007). Concatenated metallothionein as a clonable gold label for electron microscopy. J. Struct. Biol. *160*, 70–82.

Miller, M.D., Farnet, C.M., and Bushman, F.D. (1997). Human immunodeficiency virus type 1 preintegration complexes: studies of organization and composition. J. Virol. *71*, 5382–5390.

Miyauchi, K., Kim, Y., Latinovic, O., Morozov, V., and Melikyan, G.B. (2009). HIV enters cells via endocytosis and dynamin-dependent fusion with endosomes. Cell *137*, 433–444.

Patla, I., Volberg, T., Elad, N., Hirschfeld-Warneken, V., Grashoff, C., Fässler, R., Spatz, J.P., Geiger, B., and Medalia, O. (2010). Dissecting the molecular architecture of integrin adhesion sites by cryo-electron tomography. Nat. Cell Biol. *12*, 909–915.

Plitzko, J.M., Rigort, A., and Leis, A. (2009). Correlative cryo-light microscopy and cryo-electron tomography: from cellular territories to molecular landscapes. Curr. Opin. Biotechnol. *20*, 83–89.

Pontow, S.E., Heyden, N.V., Wei, S., and Ratner, L. (2004). Actin cytoskeletal reorganizations and coreceptor-mediated activation of rac during human immunodeficiency virus-induced cell fusion. J. Virol. *78*, 7138–7147.

Rigort, A., Bäuerlein, F.J., Leis, A., Gruska, M., Hoffmann, C., Laugks, T., Böhm, U., Eibauer, M., Gnaegi, H., Baumeister, W., and Plitzko, J.M. (2010). Micromachining tools and correlative approaches for cellular cryo-electron tomography. J. Struct. Biol. *172*, 169–179.

Sartori, A., Gatz, R., Beck, F., Rigort, A., Baumeister, W., and Plitzko, J.M. (2007). Correlative microscopy: bridging the gap between fluorescence light microscopy and cryo-electron tomography. J. Struct. Biol. *160*, 135–145.

Schwartz, C.L., Sarbash, V.I., Ataullakhanov, F.I., McIntosh, J.R., and Nicastro, D. (2007). Cryo-fluorescence microscopy facilitates correlations between light and cryo-electron microscopy and reduces the rate of photobleaching. J. Microsc. *227*, 98–109.

van Driel, L.F., Valentijn, J.A., Valentijn, K.M., Koning, R.I., and Koster, A.J. (2009). Tools for correlative cryo-fluorescence microscopy and cryo-electron tomography applied to whole mitochondria in human endothelial cells. Eur. J. Cell Biol. *88*, 669–684.

Wang, Q., Mercogliano, C.P., and Löwe, J. (2011). A ferritin-based label for cellular electron cryotomography. Structure *19*, 147–154.

Wright, E.R., Schooler, J.B., Ding, H.J., Kieffer, C., Fillmore, C., Sundquist, W.I., and Jensen, G.J. (2007). Electron cryotomography of immature HIV-1 virions reveals the structure of the CA and SP1 Gag shells. EMBO J. *26*, 2218–2226.

Wu, X., Anderson, J.L., Campbell, E.M., Joseph, A.M., and Hope, T.J. (2006). Proteasome inhibitors uncouple rhesus TRIM5alpha restriction of HIV-1 reverse transcription and infection. Proc. Natl. Acad. Sci. USA *103*, 7465–7470.

Zhang, P., Khursigara, C.M., Hartnell, L.M., and Subramaniam, S. (2007). Direct visualization of Escherichia coli chemotaxis receptor arrays using cryo-electron microscopy. Proc. Natl. Acad. Sci. USA *104*, 3777–3781.

Zhang, P., Bos, E., Heymann, J., Gnaegi, H., Kessel, M., Peters, P.J., and Subramaniam, S. (2004). Direct visualization of receptor arrays in frozen-hydrated sections and plunge-frozen specimens of E. coli engineered to overproduce the chemotaxis receptor Tsr. J. Microsc. *216*, 76–83.